

Analysis of the Force Applied to Stump Support in Single-Legged Para-cycling

Kenny Cho

Supervisors: Dr. David Hobbs & Professor Mark Taylor

Co-supervisors: Dr. David Haydon & Ms. Lauren Wearne

This thesis is submitted to the College of Science and Engineering in partial fulfilment of the degree of Master of Engineering (Biomedical), Flinders University – Adelaide, Australia

 Date: 2021.11.12
16:18:48 +10'30' Dr David Hobbs

I have provided feedback on this document and the student has implemented it fully.

Declaration

I certify that this thesis does not incorporate, without acknowledgement, any material previously submitted for a degree or diploma in any university, and that to the best of my knowledge and belief it does not contain any material previously published or written by another person, except where due reference is made in the text.



.....

Kenny Cho

Acknowledgements

First, I would like to bring my supervisors, Dr. David Hobbs, and Professor Mark Taylor forward, and thank them for their guidance and support throughout this project. Both have shared the value of research and the meaning of improving human health. I am truly humble to be mentored by them.

I would like to thank Dr. David Haydon from South Australian Sports Institute for providing industry insights and general testing equipment on the project to successfully execute the study. I would like to thank Ms. Lauren Wearne as co-supervisor in this project, providing mentorship and guidance in the process of study.

I would like to thank Richard Stanley and Craig Dawson from CSE Engineering Services for helping with the experimental testing setup and data acquisition.

I would also like to thank Mr. Leo Rodgers for providing professional insights and personal stories of Para-Cycling in the beginning of the study through years of professional cycling in the Paralympics.

And lastly, I would like to thank Mrs. Aisha Pejic-Cho, who has gone through this academic journey, keeping me grounded while providing indescribable support throughout the year right beside me.

Table of Contents

Abstract

Introduction

1. Biomechanics of Cycling

1.1. Kinematics

1.1.1. Mechanical Force Generation

1.1.2. Force and Strain Relationship

1.2. Major Muscle Groups of Cycling

1.3. Muscle Activation Pattern

2. Literature Review

2.1. Kinematics of Single-legged Para-cycling

2.2. Muscular Activation

2.3. Limitations

3. Project Aims

3.1. Study Objectives

4. Finite Element Analysis (FEA)

4.1. Methods and Materials

4.2. FEA Protocol

4.2.1. Mesh Parameters

4.2.2. Boundary Conditions

4.3. FEA Results

5. Experimental Test

5.1. Verification Testing Setup

5.1.1. Strain Gauge

5.1.2. Strain Analysis

5.1.3. National Instruments

5.1.4. Experimental Protocol

5.1.5. Data Processing

5.1.6. Identifying Signals of Interest

5.2. Verification Results

5.2.1. Applied Force and Strain Verification

5.2.2. Theta and Strain Verification

5.2.3. Comparison between FEA and Experimental Test

6. Discussions

7. Future Work

8. Conclusion

References

Appendix

Abstract

Current studies have highlighted the importance and attributes of pedalling movement in relation to the performance of able-bodied cyclists. The coordination of an able-bodied cyclist's pedalling movement, which consists of pushing and pulling actions, is well understood; lower extremity joints and related muscle groups work to rotate the crank via pedals. However, a para-cyclist with amputation of one-leg performs both the pushing and pulling action by a unilateral leg. Despite the information on the neuromuscular activation pattern of a single-legged amputee's pedalling motion, there is still a lack of research on amputee cyclists who utilise a stump support during cycling, competing in different classifications. The main purpose of this study is to develop a protocol to assess the force applied on the stump support during cycling. The first objective is to establish a relationship between the force applied to the stump support during cycling. Finite element analysis (FEA) will be performed to propose a viable location for the strain gauges to be placed. Experimental study will be conducted to verify this location. The second objective is to use the measured strain to derive the direction of the force applied to the stump support. This allows for the characteristics of the force to be identified in terms of direction. FEA results showed that there was a relationship between the force applied onto the stump support, and the strain found on the stump support. Following the FEA, this observed linear relationship was verified during experimental testing. Both the FEA and the experimental study showed that there is a linear relationship between the maximum strain and the angle between forces applied to the stump support. The establishment of this relationship further indicates that the direction of the force being applied to the stump support during cycling can be derived by analysing the strain on the stump support. This method will allow for identification of the direction that the force is applied onto the stump support.

Introduction

Since the introduction of bicycles in 20th century by French engineers, Michaux and Lallement, millions of people have been using bicycles for a mode of transportation, recreationally or competitively. Following this, with the arrival of a stationary bicycles (cycle ergometers), physiotherapists and rehabilitation specialists were able to further test the physical fitness of a cyclist and perform applied physiology research to better understand lower extremity movements. Furthermore, the astute understanding of “standard” activation patterns of lower limb muscles has enabled scientists and coaches to focus on a particular phase of pedalling action to train specific muscle groups [1].

Current studies have highlighted the importance and attributes of pedalling movement in relation to the performance of able-bodied cyclists. The coordination of an able-bodied cyclist’s pedalling movement, which consists of pushing and pulling actions, is well understood; lower extremity joints and related muscle groups work to rotate the crank via pedals. However, a para-cyclist with amputation of one-leg performs the aforementioned pedalling movement by a unilateral leg. One study investigated the pedalling technique related to neuromuscular activation in order to improve pedalling efficiency and performance of a single-legged amputee cyclist, reporting that it is different than that of two-legged-able-bodied cyclist [2].

Despite having such information on the neuromuscular activation pattern of a single-legged amputee’s pedalling motion, there is still a lack of research on amputee cyclists who utilise a stump support during cycling, competing in a different classification. Additionally, this is a case study which cannot constitute a global generalisation; hence, there is still a need to understand this cycling technique in greater detail.

The stump support is a structure attached to the bicycle in which para-athletes place their amputated leg, holding and supporting the cyclist. How the stump support is utilised in cycling has not been investigated, which has hindered the possibility of performance improvement and rehabilitation for para-cyclists.

According to Union Cyclists International (UCI), para-cyclists with a physical impairment who utilise a stump support compete in the C2 classification [3]. These

para-cyclists present with single above knee amputation with no prosthesis but may use a stump support. These para-cyclists may use bicycles, in which one side is equipped with a pedal while the other side is equipped with a stump support without a pedal as shown in Figure 1.



Figure 1. Bicycle Setup of a Para-cyclist: Stump support on the Left, Pedal on the Right [Image adapted from The Courier]

The execution of the 'start-up' phase of cycling has been reported to strongly correlate with the overall race performance [4]. During this phase, cyclists are fixed at the starting line and must accelerate to their top speed as quickly as possible. This phase is not only crucial for para-athletes during a race, but is an area of research interest when analysing cycling kinematics, due to the large amount of movement of the cyclist. For example, able-bodied cyclists emphasise their hip joint movement at the start-up phase to maximise the degree of freedom, and consequently, produce maximum momentum [5]. Comparatively, the kinematics during the start-up phase for single-legged para-cyclists is currently unknown, especially when utilising a stump support. Coaches have

observed that using a stump support may substantially constrain hip movement, forcing para-athletes to produce limited momentum at the start-up phase [6].

This study has the potential to broaden the understanding of para-cycling for general audiences, who may or may not be elite cyclists.

The purpose of this study is to develop a protocol to assess the force applied on the stump support during cycling. These findings act as a foundation for further investigation on single-legged para-cyclists' pedalling technique and neuromuscular activation pattern while using a stump support.

Chapter 1: Biomechanics of Cycling

The biomechanics of cycling is a complex motion that involves various muscle groups and joints. To understand such a complex motion, the fundamentals of cycling need to be addressed. This chapter presents the main skeletal muscle groups of the lower limbs that are used during cycling, followed by the biomechanics involved in cycling.

1.1. Kinematics

The term 'pedalling' in cycling refers to a cyclic motion propelled by flexion and extension of the lower limbs, which is also known as the crank cycle. This crank cycle can be broken into four main sections, starting from the top as shown in Figure 1. To note, the angle 0° , relates to the position of the foot relative to the TDC in the crank cycle. Top Dead Centre (TDC) refers to the position of a foot at the top of the pedal stroke.

At the TDC, the hip, knee and the ankle joints are all in maximal flexion. The foot on the pedal is at the top of the cycle. Following this, the Push-downstroke phase begins with leg extension until the foot reaches the bottom of the cycle and the leg is extended maximally, reaching BDC. At the BDC phase, the position at which the foot is relative to the initial position is 180° . Following the BDC phase, the leg goes into flexion once more to reach up to the top of the cycle, towards TDC.

Numerous studies have described the relationship between the 'active' leg and 'passive' leg during cycling, which respectively relates to the pushing phase, and the pulling phase [7]. During the pulling phase of cycling between 180° and 360° , the passive limb flexes to reduce its resistance on the crank to allow propulsion on the contralateral limb, entering the pushing phase [8]. In other words, the two limbs are coupled by the cranks and are 180° out of phase, in which one limb is in pushing phase, pedalling the crank downward while the other limb is in pulling phase.

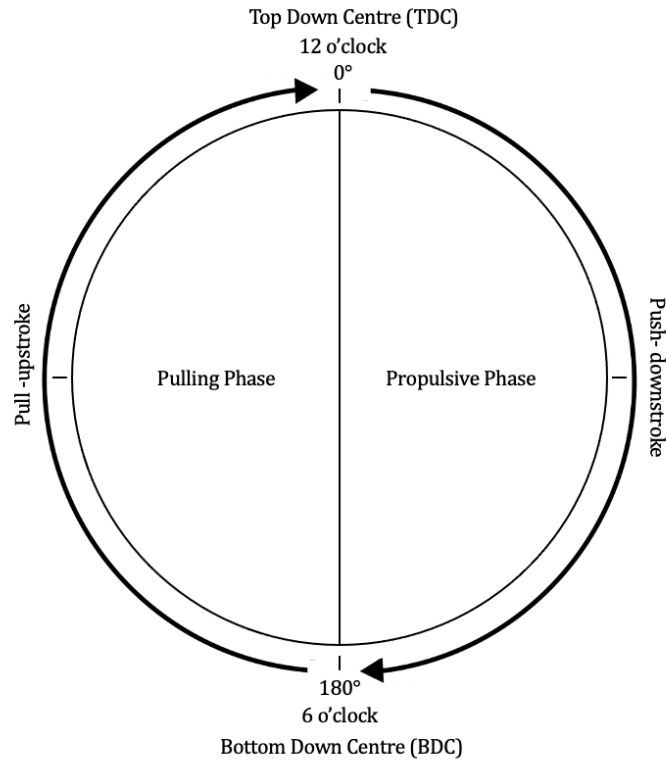


Figure 2. Crank Cycle and Phases of a Pedalling Motion

1.1.1 Mechanical Force Generation

Crank torque is defined as the product of the force perpendicular to the crank arm and its crank's length found at different phases of a crank cycle. This dynamic torque is the key factor of pedalling motion in propelling the bicycle forward [9].

The revolution of the crank during cycling is primarily generated by a tangential force (F_T) that is applied perpendicular to the crank arm of a bicycle (Figure 3) while centrifugal force (F_C) provides minimal contribution to the rotation of the pedal [9]. Furthermore, the resultant forces throughout the revolution of the crank highlight the contribution of tangential forces in various phases of the crank cycle to provide optimal performance. Finally, the tangential force is negative (directed opposite to the pedalling motion) during the pulling (between 195° and 360°) phase of the cycle, which suggests that the greatest force is generated by the contralateral leg in pushing phase [10].

The physical setup of a bike allows the pedals to be 180° out of phase for able-bodied cycling, where the leg in the upstroke phase is raised by the contralateral leg, which is in the downstroke phase of the cycle.



Figure 3. Overview of major forces at the pedal in the downstroke phase of 90°. (M=propulsive torque, F_c=centrifugal force, F_t=tangential force) [Image adapted based on Fonda, B, 2010]

1.1.2. Force and Strain Relationship

In relation to force during cycling, the force exerted on the pedal to rotate the crank is observed during the pushing phase of the crank cycle by an 'active limb'. This applied force can be expressed in terms of strain by the relationship between stress and strain.

Force can be expressed in many ways, depending on the application of the situation. For example, when a force is applied perpendicular or 'normal' to a surface of an object, a normal stress is observed by that object. Unconditionally, objects under stress observe strain. Strain is a unitless measurement that is defined as a ratio between lengths. By plotting stress against strain, the behavior of an object can be described. Therefore, force applied to a surface can be expressed as stress and can be derived from strain. Furthermore, depending on the material properties of an object, the relationship between stress and strain can deduce the characteristics of a material [11].

1.2. Major Muscle Groups of Cycling

Cycling motion predominantly occurs in the sagittal plane, driven by flexor and extensor muscles of the lower limbs, performing a cyclic movement of flexion and extension [12]. Studies have indicated the following single-joint muscles as the most active muscles during cycling (Figure 3): Gluteus Maximus (Gmax), Gluteus Medius (GM), Vastus Lateralis (VL), Vastus Medius (VM), Tibialis Anterior (TA) and Soleus (SOL). Two-joint muscles include: Rectus Femoris (RF), Semimembranosus (SM), Semitendinosus (ST), Bicep Femoris (BF), Gastrocnemius Lateralis (GL), and Gastrocnemius Medialis (MG).

Image removed due to copyright restriction.

**Figure 3. Major superficial muscles of the lower limb -anterior (left) and posterior (right) views
[Image adapted from Bourke, et al, 2013]**

The above muscles can be separated into the following major muscle groups based on their location and functional activity in relation to the crank cycle as shown in Table 1 below:

Table 1: The function and location of major muscles of the lower limb (adapted from [7])

List of Major Muscles			
Muscle	Location	Functions	Active Phase
Gluteus maximus	Gluteal region (superficial)	- Hip extension - Hip lateral rotation - Hip abduction	Between 340° and 80°.
Biceps femoris	Hamstring (posterior)	- Knee flexion - Hip extension	Between 350° and 230°. Peak at 110°.
Semimembranosus & Semitendinosus	Hamstring (posterior)	- Knee flexion - Hip extension	Between 10° and 230°.
Rectus femoris	Quadriceps (anterior)	- Knee extension - Hip Flexion	Between 200° and 110°.
Vastus lateralis. medialis	Quadriceps (anterior)	- Knee extension	Between 330° and 120°.
Gastrocnemius medialis/ lateralis	Calves (posterior)	- Talocrural joint stabilisation - Knee flexion	Between 25° and 260°.
Soleus	Calves (posterior)	- Talocrural joint stabilisation	Between 340° and 270°.
Tibialis anterior	(anterior)	- Talocrural joint stabilisation - Ankle stability	Throughout the cycle, peak at 280°

1.3. Muscle Activation Pattern

Forementioned muscles play a major role in cycling as they contribute to the generation of the force required to turn the pedal, which in turn, propels the bicycle forward. The muscle activation pattern of these muscle in relation to the crank cycle is shown in Figure 4. These activation patterns in synchronisation with the kinematics have been developed and understood for able-bodied cyclists. This establishment has allowed for greater understanding of how they contribute to force generation.

However, their activation patterns are currently unknown for single-legged para-cyclists who utilises a stump support. Resultantly, their force generation with the potential for performance enhancement, is currently also unknown.

Image removed due to copyright restriction.

Figure 4. Overview of muscle activity timing during cycling in relation to the crank cycle: 1) TA, 2) SOL, 3) GM, 4) VL&VM, 5) RF, 6) BF, 7) Gmax [3] [Image adapted from Biomechanics of Cycling by Fonda, B, 2010]

Chapter 2: Literature Review

2.1. Kinematics of Single-legged Para-cycling

Peddalling movement of cycling has been profoundly investigated with respect to the relationship between muscle activation and crank position for 'abled-bodied' cyclists. The understanding of this activation pattern has enabled scientists and trainers to focus on a particular phase of pedalling action to train specific muscle groups [13]. The same understanding and potential performance benefits have not been extended to para-cyclists.

Para-cyclists with a single leg amputation perform the pedalling movement on bicycle by unilateral leg, acting as the both the active and passive limb in relation to the crank cycle. Therefore, different neuromuscular activity patterns are observed [2]. This study showed that neuromuscular activation of RF muscles increased during the entire pulling phase for single-legged para-cyclists while the same muscles were only active during latter half of the pulling phase for able bodied cyclists. Following this, the author noted that joint torques during this phase were highly emphasized in the hip flexion joint moment for single-legged para-cyclists as this may be compensation for a lack of hip and/or knee extension torque from the contralateral leg.

Furthermore, analysis between the activation of lower extremity muscles against the workload was investigated to qualitatively assess the effect of increase in workload on the activity of each muscle and to estimate their roles during cycling. The results showed that, specifically, there was no increase in activity in RF muscles with the increase in workload for para-cyclists [2] while other muscles, such as VL consistently increased with an increase in workload. This positive linear relationship between the muscle activity and the workload reflected muscle's contribution to generate crank force for increasing workload. Thus, it was concluded that RF muscles could not contribute to generate crank force, rather, they act to pull up the leg [2].

One study noted that single-leg cyclists elicit a comparatively greater pulling action than two-leg cycling [14]. An explanation for this is the power, produced by the contralateral-leg to rotate the latter half of the crank cycle during pulling action, is

absent for single-legged cycling. Instead, flexor muscles are activated to pull the leg back up to overcome the propulsive torque generated during the pushing action [14]. Further analysis investigating the pedalling technique reported that there was an increase in hip and knee flexion-joint torques when the cyclists applied a pedal-force that is perpendicular to the crank arm during single-leg cycling [15]. This observation showed that the activation of the hip and knee flexor muscles was activated during the pulling action, which supported the former explanation [15].

2.2 Limitations of Current Studies

The usage of a stump support in terms of force generation has not been investigated. Such potential for force generation on the stump support occurs through both pushing and pulling action of the hip flexor, which is connected to the residual stump. One study highlighted the differences between abled-bodied cyclists and cyclists with transtibial amputation (CTA) in terms of their biomechanics during cycling [15]. This study showed that cyclists with CTA, during the pulling phase, could not efficiently stabilise their ankle for force transfer from hip flexor muscles nor could they dorsiflex their ankle for clearance of the contralateral leg during TDC phase of the crank cycle. The contribution of prosthetic ankles in effectively executing the pulling phase was also minute thus creating a need for accommodation through increased hip and knee flexion. Furthermore, the study highlighted that attempting to 'pull up' during this phase increased the total forces seen at the pedal, but also increased metabolic cost. Following this, the author provided recommendations for prosthetic design for future para-cyclists [15]. Although this study showed quantifiable measurements for transtibial para-cyclists with a prosthetic ankle, further investigation is required to understand the biomechanics of transfemoral para-cyclists who utilise a stump support.

Overall, limited attention to date has addressed the effect of stump support during cycling with trans-femoral amputation. This study hopes to develop a technique, which will allow for a deeper understanding of single-legged cycling by investigating the biomechanics of para-cyclists with a transfemoral amputation, who utilise stump supports.

Chapter 3: Project Aims

The overall aim of this study is to understand the pedalling technique of single-legged Para-Cycling when utilising a stump support. Execution of the following objectives will allow for this aim to be fulfilled.

3.1. Study Objectives

The main objective of this study is to develop a reliable and repeatable method to assess force applied to the stump support during single-legged para-cycling.

The first objective is to establish a relationship between the force applied to the stump support during cycling. Finite element analysis (FEA) will be performed to propose a viable location for the strain gauges to be placed. Experimental study will be conducted to verify this location.

It was assumed that the measurement of strain by the strain gauge, placed in the viable location on the stump support, can be used to derive the applied force.

The second objective is to use the measured strain to derive the direction of the force applied to the stump support. This allows for the characteristics of the force to be identified in terms of direction.

Chapter 4: Finite Element Analysis (FEA)

4.1. Methods and Materials

Ansys Workbench (2020) software was used to perform FEA on the stump support to locate the placement of strain gauges with aims to derive the force applied to the stump support when cycling by analysing the observed strains.

To address the first objective of this study, the Stump Support was selected as the instrument of FEA because a large deflection of the stump support was observed during the pulling phase of the healthy limb. This implied that the para-cyclist was applying a degree of force onto the stump support to efficiently execute the crank rotation. To address the second objective, an analysis of strains found on the stump support was used to derive the force applied by the para-athlete.

A model of the stump support shown in figure 5 below was provided by South Australian Sports Institute (SASI) and was imported as a .stl file to Ansys Workbench software.

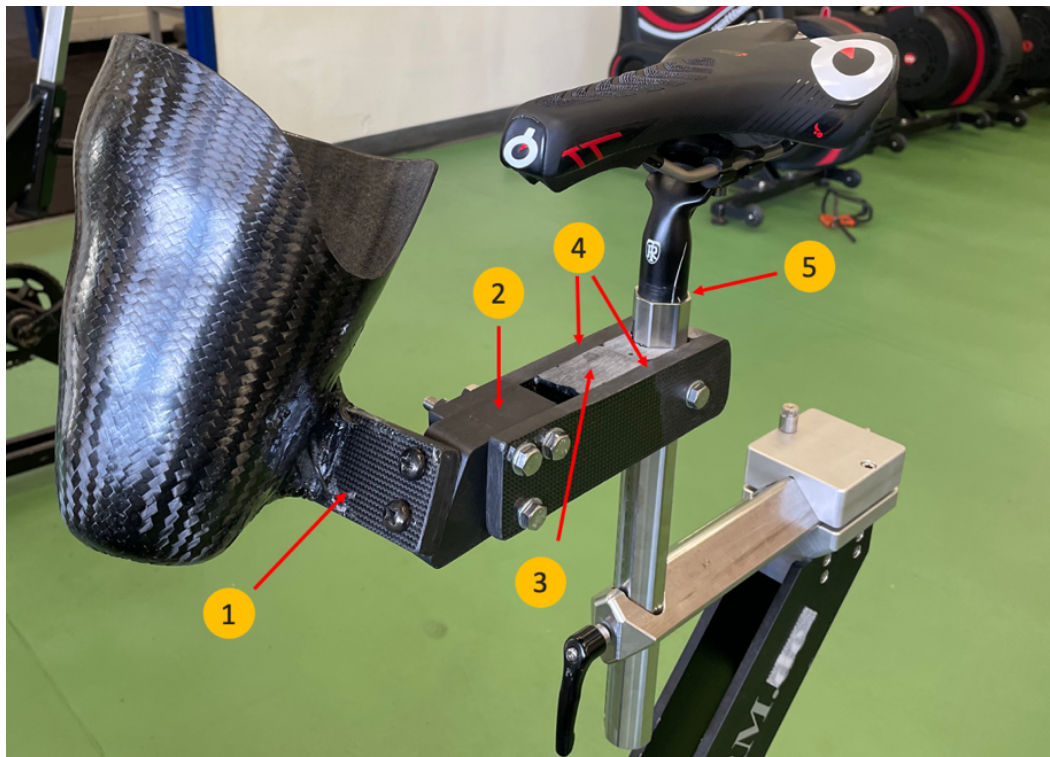


Figure 5. Training Bike with a Stump Support with different parts labelled; 1. Front plate, 2. Bridge plate, 3. Rear plate, 4. Outer plates, 5. Bike seat pole [image obtained from SASI, 2021]

Assumptions:

1. The material of stump support part 1, 3 and 4 are all pure carbon fibre, part 2 is Onyx™, which is a carbon infused nylon [16].
2. The bolts are all stainless steel.
3. The force observed in the prosthetic socket of the stump support is translated to the Front Plate of the stump support; force is applied at the front plate in the analysis.
4. Front plate and bridge plate are joined by two stainless steel bolts and corresponding nuts; there's a space between the bolts and threaded inner surface of two plates.
5. Application of adhesive (i.e., glue) between the strain gauge to the plates does not affect the material properties of the plates.

4.2. FEA Protocol

4.2.1. Mesh Parameters

To determine the optimal mesh size for the model construct, mesh convergence was performed and plotted as shown in Appendix A. The mesh convergence plot (Appendix A) showed that the element size of 0.002m with Tetrahedral method with Quadratic element order produced the optimal mesh for the model. The mesh analysis resulted in a total number of 179286 Nodes and 103009 Elements (Appendix B).

4.2.2. Boundary Conditions

Boundary condition of the analysis was determined based on the assumptions made of the stump support and its use during cycling. These boundary conditions were critical in performing finite element analysis.

The rear surface of the bridge plate was selected as the fixed constrained point by applying 0m displacement on all X, Y, and Z directions. This rear surface was selected as the fixed point based on its proximity to the bike seat that provides the stability to the whole system. Following this, a force of 700N was applied at the vertex of the front plate in Y and Z directions as shown in Figure 6. The magnitude of the force was determined based on the weight of the para-cyclist (70kg), where it was assumed that the para-cyclist applied their full body weight onto the stump support. The direction of the force

was determined to be tangential and centrifugal based on the way the force is applied to the pedal to rotate the crank cycle of an able-bodied cyclist.

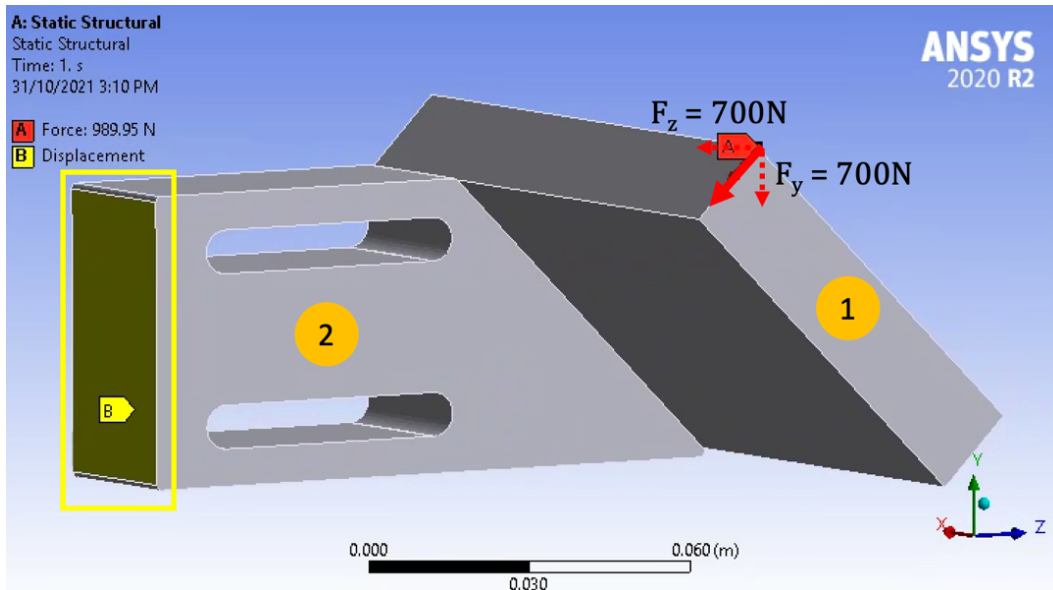


Figure 6. Boundary Condition of the Stump Support Model: Displacement (Yellow), Force (Red)

4.3. FEA Results

Initial analysis was performed to the overall model to determine surface areas with the maximum strain when applying a force as shown in Figure 7.

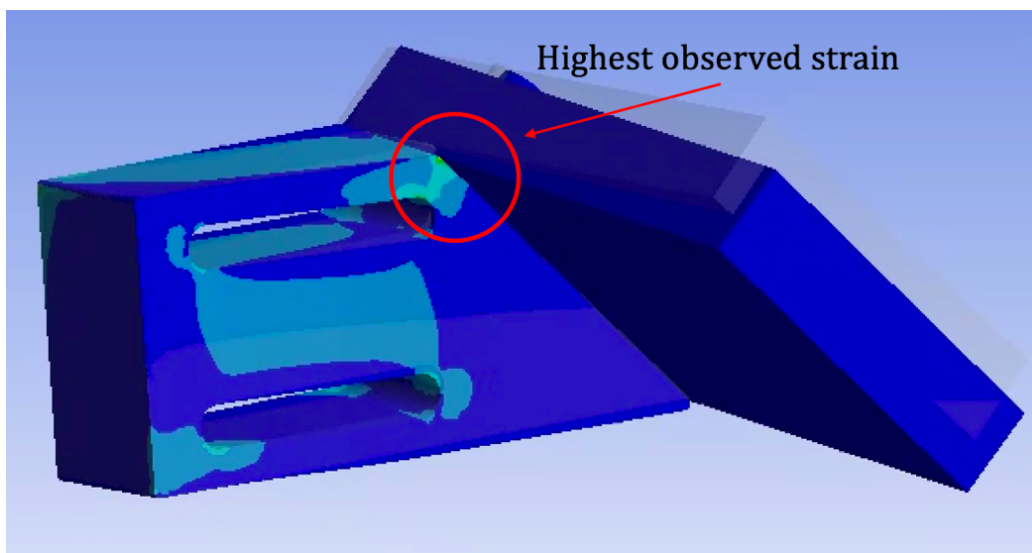


Figure 7. Maximal Principal Elastic Strain Results of the Model: Front plate & Bridge plate

Based on the initial analysis of the overall model, the surface area next to the bolt-slot holes showed the highest strain values. When further analysing the strain of the internal component, the two bolts connecting the front plate and the bridge plate showed the largest strain (Figure 8). Further analysis was performed to determine the type of relationship between the strain found on the bolts and the force applied at the front plate.

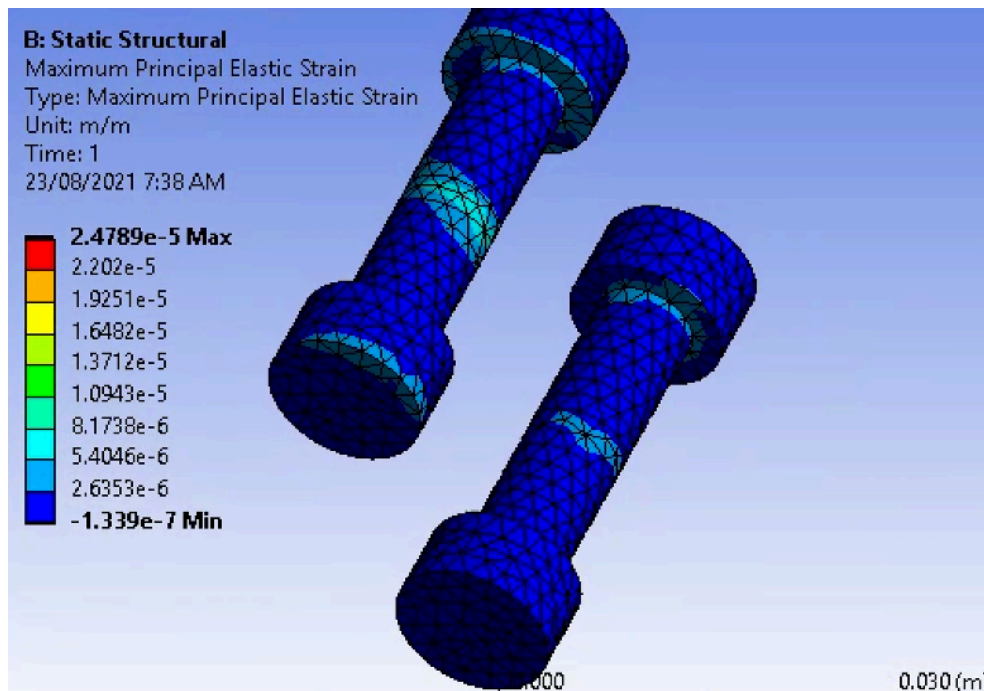


Figure 8. Maximal Principal Elastic Strain Results of the Bolts

Following this, the relationship of the strains found between top bolt and the bottom bolt during force application was investigated by analysing the angle (θ) between two forces applied in Y, and Z directions, called theta. This variable was introduced to understand how the strain found on the bolts, changes with the direction of the applied force. This understanding was necessary to describe how the force was being applied to the stump support, and ultimately inferring the usage of such device. Furthermore, the differences in maximum principal strain between two bolts were calculated to further determine the direction of the force being applied to the bolts. The result of this analysis is as shown in Table 2.

Table 2. Forces Applied in Y, Z Directions with Corresponding Angle Between Two Forces, and Maximum Principal Strain: P25 – Force Applied in Y Direction, P26 – Force Applied in Z Direction, P23 – Maximum Principal Elastic Strain Found at the Top Bolt, P24 – Maximum Principal Elastic Strain found at the Bottom Bolt

P25 - Force Y Component	P26 - Force Z Component	P23 - Maximum Principal Elastic Strain (top) Maximum	P24 - Maximum Principal Elastic Strain (bottom) Maximum	Theta	Differences in Max Principal Strain
N	N	m m ⁻¹	m m ⁻¹		
-700	0	1.71E-05	6.29E-06	0	1.08E-05
-700	-100	1.66E-05	6.13E-06	8.13010235	1.05E-05
-700	-200	1.85E-05	6.47E-06	15.9453959	1.20E-05
-700	-300	2.05E-05	7.12E-06	23.19859051	1.34E-05
-700	-400	2.26E-05	7.77E-06	29.7448813	1.49E-05
-700	-500	2.48E-05	8.42E-06	35.53767779	1.63E-05
-700	-600	2.69E-05	9.07E-06	40.60129465	1.78E-05
-700	-700	2.90E-05	9.73E-06	45	1.93E-05

The results showed that there was a linear relationship between the differences in maximum principal strain and the angle between two forces applied on the bolts. Additional sets of force were applied to further investigate this linear relationship, ultimately to verify such relationship was observed with changes in the magnitude of the force applied. The result of this analysis is as shown in Figure 9. The results highlighted that analysing the strain found on the bolts was a viable solution as there was a distinct relationship between the differences in strain, and the angle between two applied forces. These results further demonstrated that the direction of the applied forces can describe the strain found on the bolts.

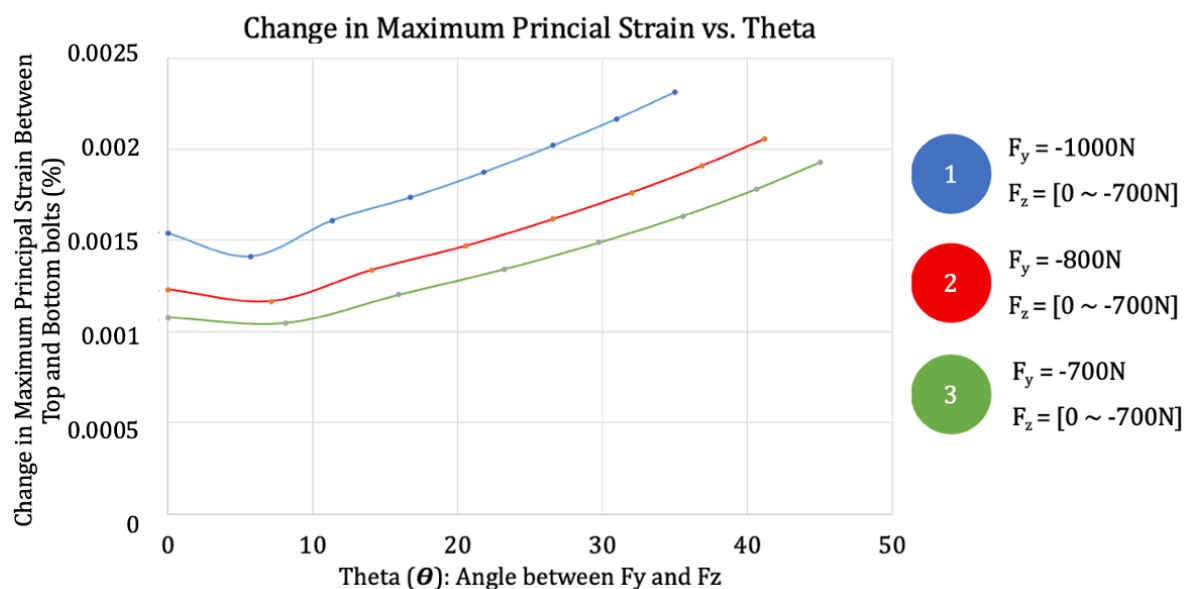


Figure 9. Differences in Maximum Principal Strain Found on the Bolts with Angle Between Forces Applied in Y, Z Directions

Although the analysis provided sufficient justification for the placement of the strain gauge on the bolts, a physical limitation was encountered. During inspection of the stump support, the bolts were fully threaded and there was no viable surface to place the strain gauge (Appendix D). This finding was in disagreement with Assumption 4.

Another solution was proposed; investigating the strain found on the surface of the bridge plate next to the bolt slot-holes. This location was selected as the next potentially viable surface based on the initial analysis shown in Figure 7. The result of this analysis is shown in Figure 10.

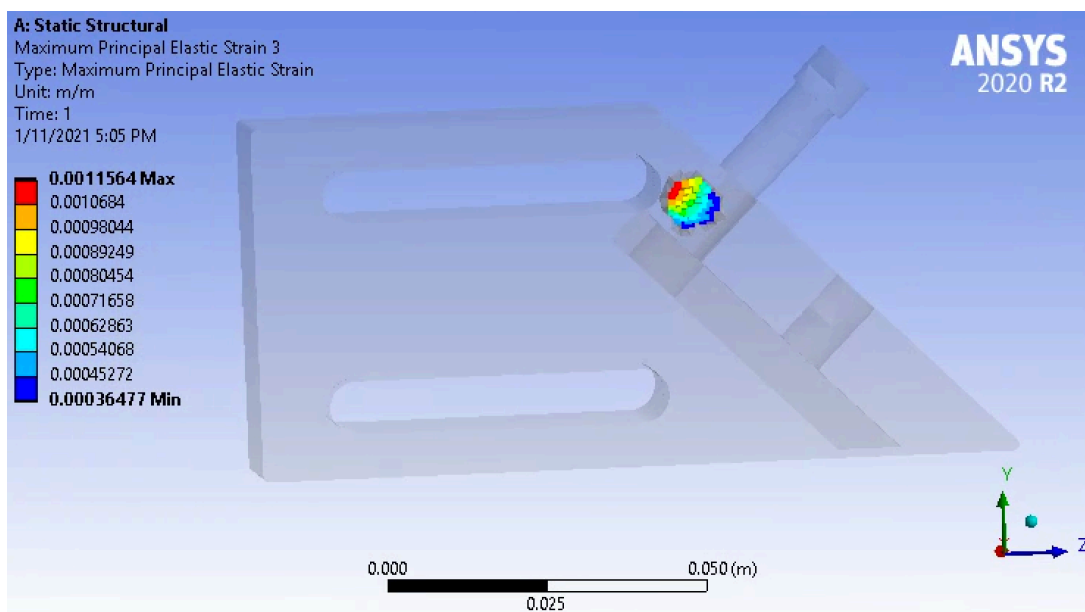


Figure 10. Maximum Principal Strain Results of the Bridge Plate: Surface Next to the Bolt Slot Holes

Similarly, the relationship between the maximum principal strain and the angle between the forces applied in the Y and Z directions was investigated. The results showed that there was a linear relationship between the principal strain and angle between forces applied in Y and Z directions as shown in Figure 11. This distinct response mechanism of the strain found on the surface of the bridge plate confirmed the proposed surface as the location for possible strain-gauge placement.

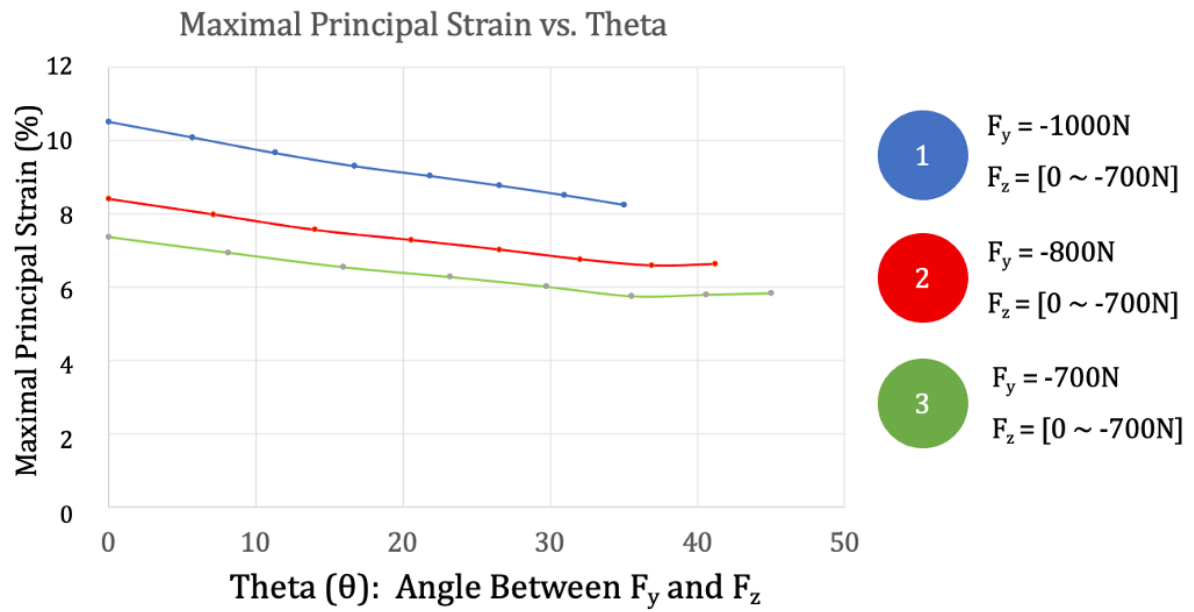


Figure 11. Principal Strain Results of the Bridge Plate

Chapter 5: Experimental Test

5.1. Verification Testing Setup

Experimental testing was performed to verify the relationship between the strain and the force applied, produced by FEA. Furthermore, this testing was able to verify the theoretically identified location for strain gauge. The verification testing was performed at the Engineering Services Workshop on Level 3 at Flinders University at Tonsley.

5.1.1. Strain Gauge

KYOWA Electronic Instruments' strain rosette from Japan was used to measure the strain of the stump support across three axes. The specification of this strain rosette is shown in Appendix C.

The KYOWA strain rosette was attached on the surface of the Bridge plate by using an adhesive glue as shown in figure 12. The illustration shown in dotted-red lines indicates the global coordinate system that the strain rosette is orientated relative to the stump support (Figure 12). Additionally, wires of the rosette were glued onto the surface of the plate to provide stability, strain relief, and minimise possible signal artifacts from the wires.

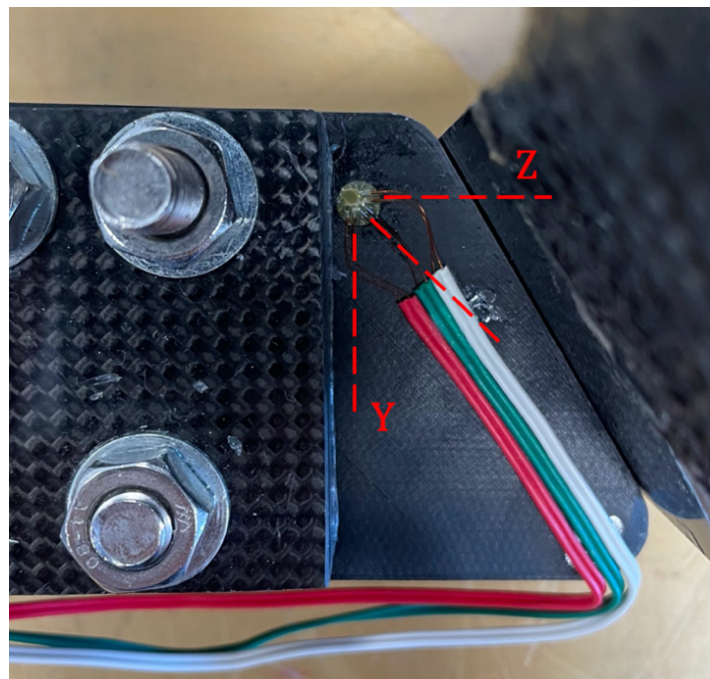


Figure 12. Strain Rosette Attachment

5.1.2. Strain Analysis

The configuration of strain rosette attached to the surface of the Bridge plate is shown in figure 13.

Image removed due to copyright restriction.

Figure 13. Strain Gauge Rosette Configuration (adapted from Kyowa Electronic Instruments: Strain Analysis)

Based on this configuration, individual maximum principal strain (ϵ) in Y and Z direction, as well as torsion (γ) in YZ direction were calculated by using the equation found in Appendix D. Furthermore, equation shown in Figure 14 was used to calculate the total maximum and minimum principal strain found on the surface of Bridge plate. To note, the strain values of ϵ_a , ϵ_b , ϵ_c , were the output measurements, directly obtained from strain analysis.

Maximum Principal Strain

$$\epsilon_{\max} = \frac{1}{2} [\epsilon_a + \epsilon_c + \sqrt{2\{(\epsilon_a - \epsilon_b)^2 + (\epsilon_b - \epsilon_c)^2\}}]$$

Minimum Principal Strain

$$\epsilon_{\min} = \frac{1}{2} [\epsilon_a + \epsilon_c - \sqrt{2\{(\epsilon_a - \epsilon_b)^2 + (\epsilon_b - \epsilon_c)^2\}}]$$

Figure 14. Maximum/Minimum Principal Strain Equation (adapted from [17])

5.1.3. National Instruments

National Instruments SignalExpress tool was used to record the data and transform the analogue signals into digital signals to be analysed.

The wires of each strain gauge were configured to the three quarter-bridge strain gauge circuits as shown on the left of Figure 15. Individual strain values from ϵ_a , ϵ_b , ϵ_c , were measured from each bridge circuit, respectively. Following this, each quarter-bridge transducer was connected to the chassis as shown in Figure 15 on the right.

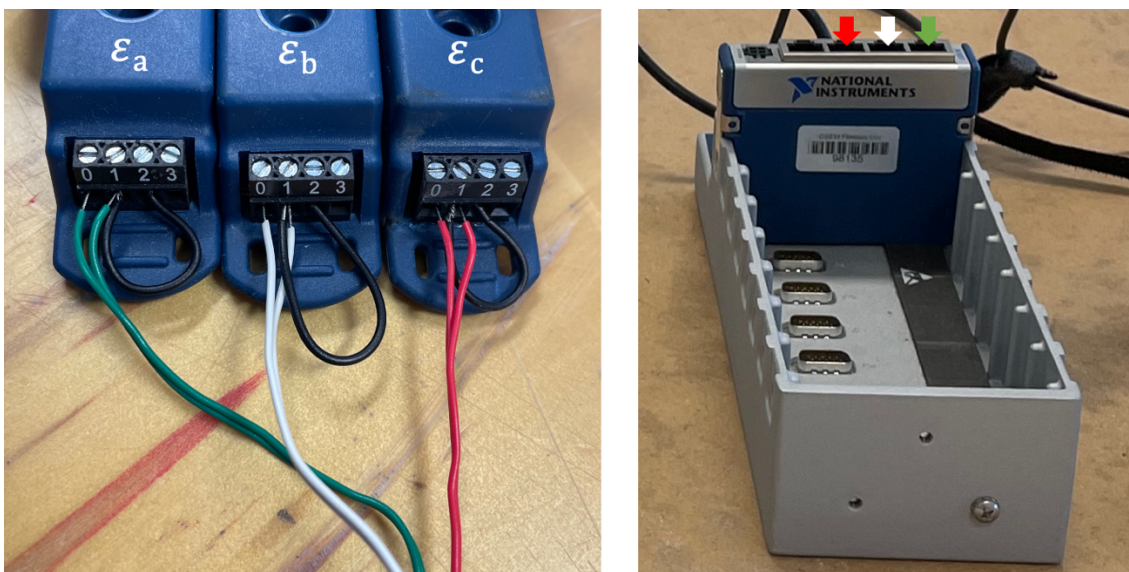


Figure 15. Strain Rosette Wiring Setup: Quarter Bridge Transducers (Left), Chassis (Right)

The coloured arrows show the input-port for each corresponding-coloured wire of the strain rosette.

SignalExpress 2015 Software was used to collect and process signals.

Input Strain

Three channels, connected from the chassis, were selected as the analogue input. Gauge factor of 2.12, and gauge resistance of 120.0Ω were selected based on the specification of the strain rosette. The V_{ex} Value of 3V, which is the supply voltage to the system, was selected based on the maximum threshold of the quarter bridge. Quarter Bridge I was selected as the strain configuration. Lastly, data was collected reading 200 samples with a rate (Hz) of 2000 (2k) as shown in Figure 16.

Zero Offset

The zero offset function was applied in the beginning of the data collection for both vertical and transverse loading tests to correctly set the zero level of the signal.

Offsetting the zero mitigated the “false” zero level of the signal as there were signal artifacts collected from the transducers.

Filter

A 2nd order lowpass Butterworth filter with a cut-off of 10Hz was applied to the data acquisition system to filter out high frequency signals collected as shown in Figure 16.

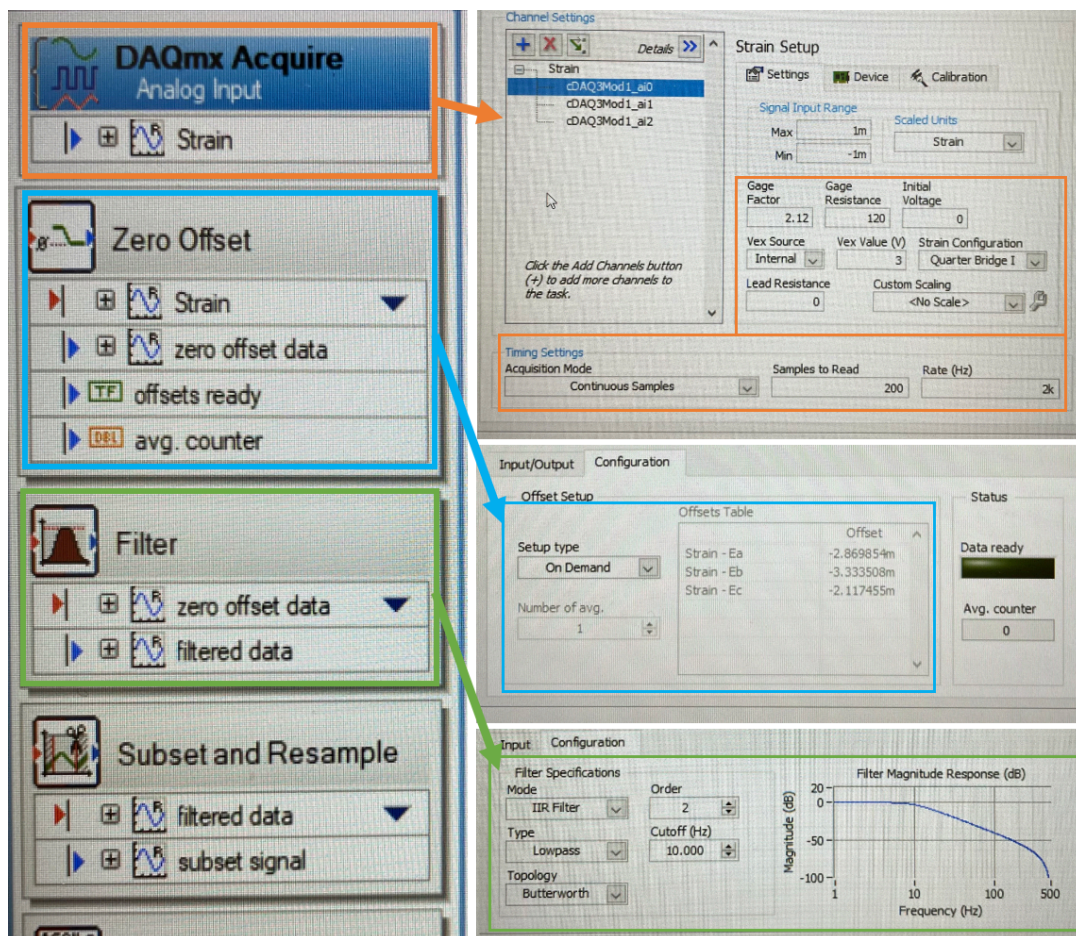


Figure 16. SignalExpress2015 Data Acquisition Setup

5.1.4. Experimental Protocol

Six 2kg weights, one 8kg cylindrical weight, and five 1kg weights with a total of 25kg weights were used to apply the force on the stump support to mimic the analysis carried out previously in FEA. The masses of the basket and chain were calibrated for during the data calibration setup.

The experimental force was applied to the stump support in two different setups to encompass both the vertical and transverse loadings as shown in Figure 17 below. The loads were applied in respect to the global coordinate system of the stump support in FEA as indicated by black circles on the bottom left corner of the figure.

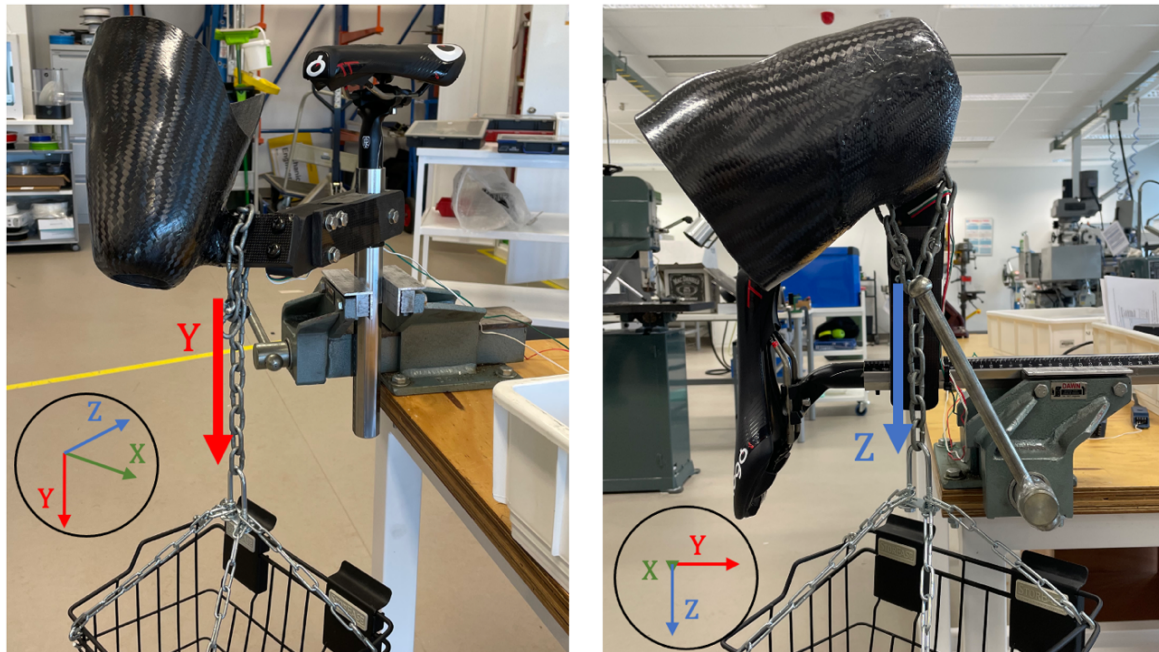


Figure 17. Experimental Load Setup: Vertical Loading Test (Left), Transverse Loading Test (Right)

In order to apply the desired force to the stump support, weights of varying mass were added as shown in Table 3. This protocol was repeated for the seven sets of force, each for one minute. A test duration of one minute was an optimal timeframe to load all the mass into the basket and collect the strain data with minimum signal artifacts observed from basket sway.

Table 3. Applied Force Calculation

Applied Force (N)	Vertical Load Test & Transverse Load Test
20	2kg
40	2 x 2kg
80	4 x 2kg
120	6 x 2kg
150	6 x 2kg + 3 x 1kg
200	1 x 8kg + 6 x 2kg
250	1 x 8kg + 6 x 2kg + 5 x 1kg

5.1.5. Data Processing

Collected data from SignalExpress 2015 software were imported to MATLAB (MathWorks, Inc.) for analysis, using custom-written scripts. Analysed strain data were imported to Microsoft Excel to be compared with the theoretical strain results from FEA.

5.1.6. Identifying Signals of Interest

The collected data from SignalExpress were expressed in strain over frame, which was segmented to obtain desired window of frames that correctly displayed the strain value when a specific force was applied. Following this procedure, strain data, collected over a duration of one minute for each set of tests, were first plotted to establish a repeatable method to extract only the frames of interests.

The method of applying the loads to the stump support created a distinct pattern of output signals when they were stack-plotted against each other. MATLAB was used to analyse the acquired data with least amount of signal artifacts. The last 100 data points of the test were selected as the signals were observed to be the most “constant” with least fluctuation as shown in Figure 18.

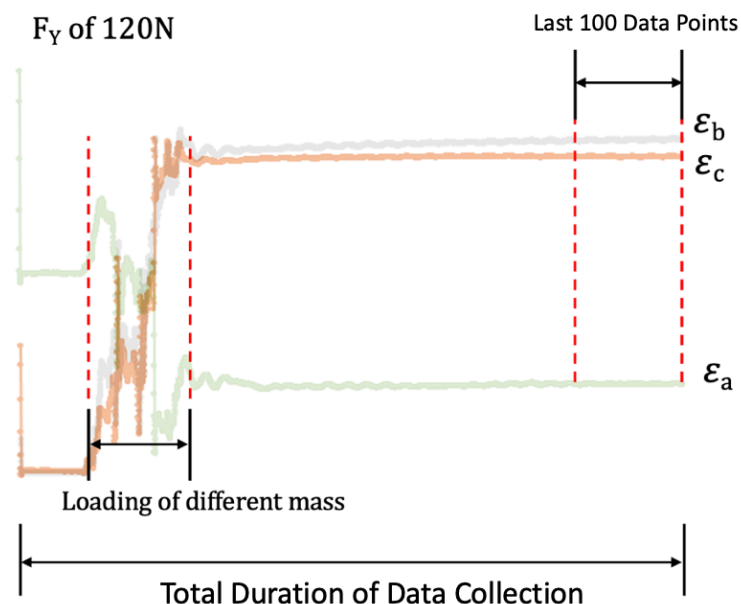


Figure 18. Identification of Suitable Individual Strain Value from Vertical Loading of 120N:

The same method was implemented for transverse load tests, extracting the last 100 data points of the collected data.

5.2. Verification Results

5.2.1. Applied Force and Strain Verification

Applied forces and observed strains for both the vertical and transverse loadings were initially analysed to verify a linear relationship between two parameters.

Experimental force vs. strain analyses verified a linear relationship between the applied force and observed strain in both the vertical and transverse load tests as shown in Figure 19.

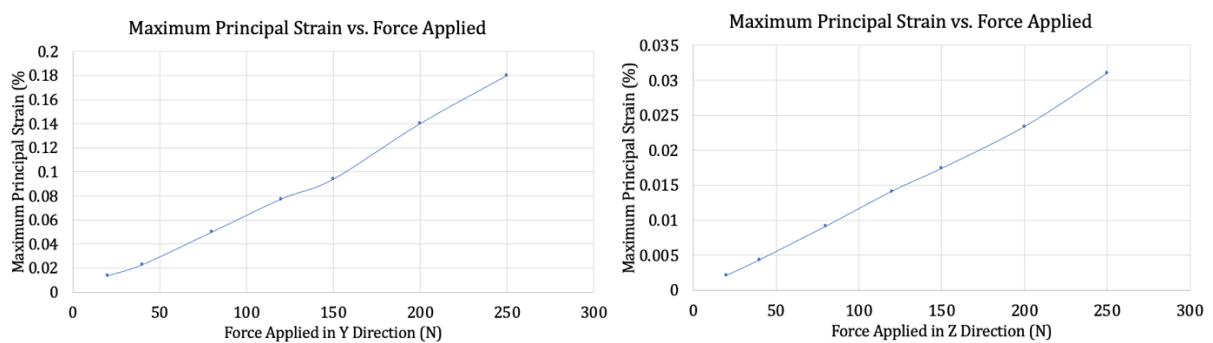


Figure 19. Maximum Principal Strain vs. Force Applied: Vertical Loading (Left), Transverse Loading (Right)

The linear relationship between applied forces and strain allowed for the Law of Superposition to be applied [18]. Bi-directional forces in linear relationship with the strain can be superposed as a resultant force as shown in Figure 20.

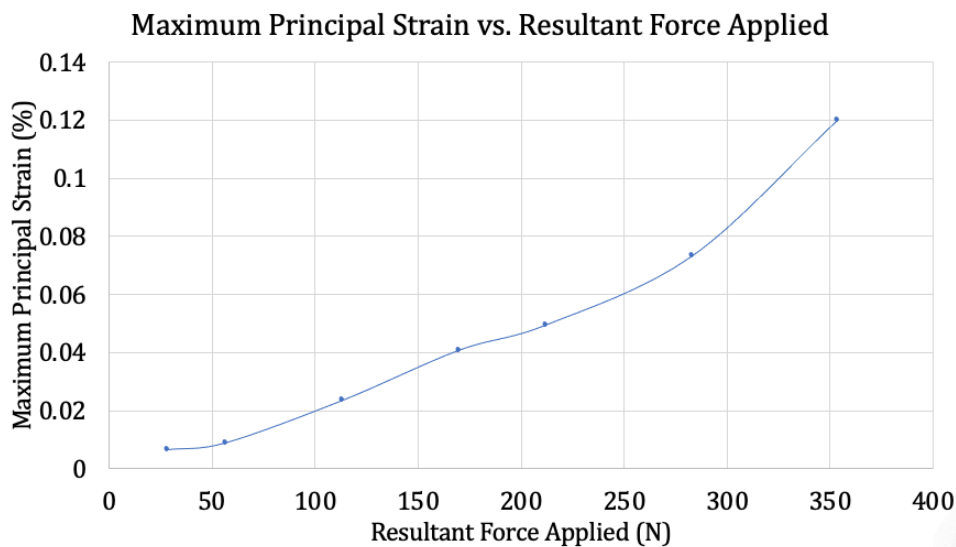


Figure 20. Maximum Principal Strain vs. Resultant Force Applied

5.2.2. Theta and Strain Verification

There was a linear relationship between the principal strain and angle between forces in Y and Z directions, which verified the results of FEA as shown in Figure 21.

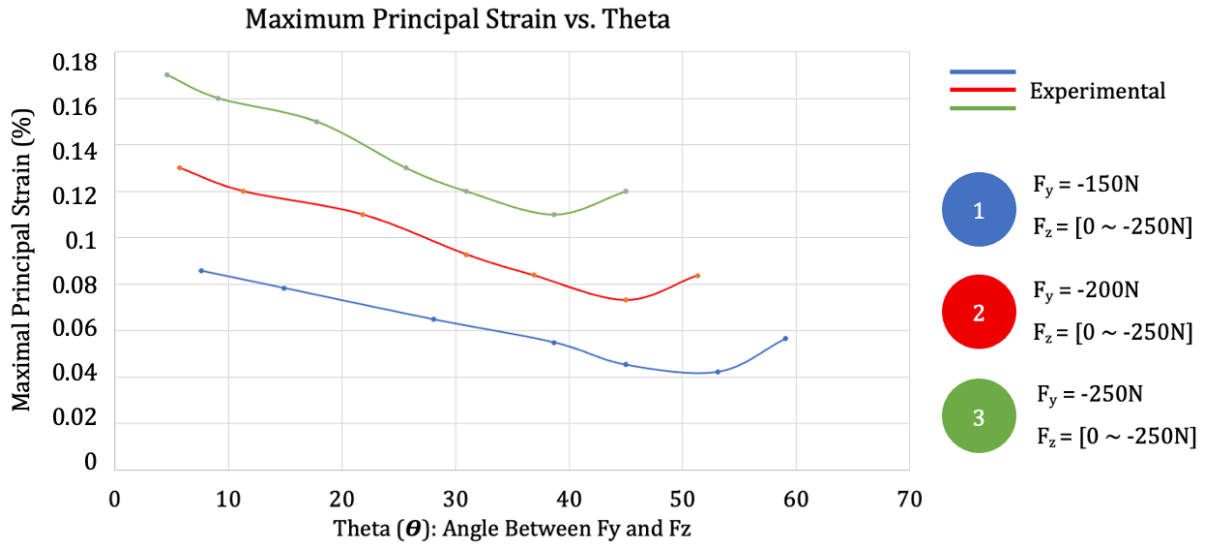


Figure 21. Maximum Principal Strain vs. Theta

The range of applied force (-700N ~ -1000N) was decreased (-150N ~ -250N) to allow for comparison of the FEA with the experimental test results. The plot showed that the theoretical results from FEA generally had a larger strain than those from experimental analysis as shown in Figure 22.

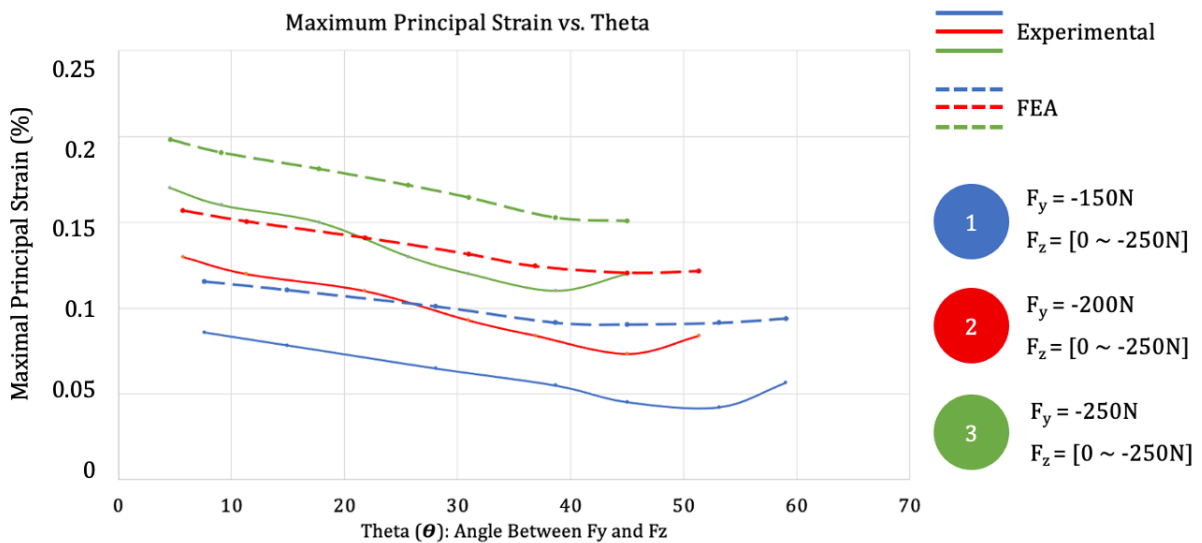


Figure 22. Maximum Principal Strain vs. Theta: Solid line (Experimental), Dashed Line (FEA)

The percent differences of strains found between the FEA results and experimental results were calculated and indicated as shown in Figure 23.

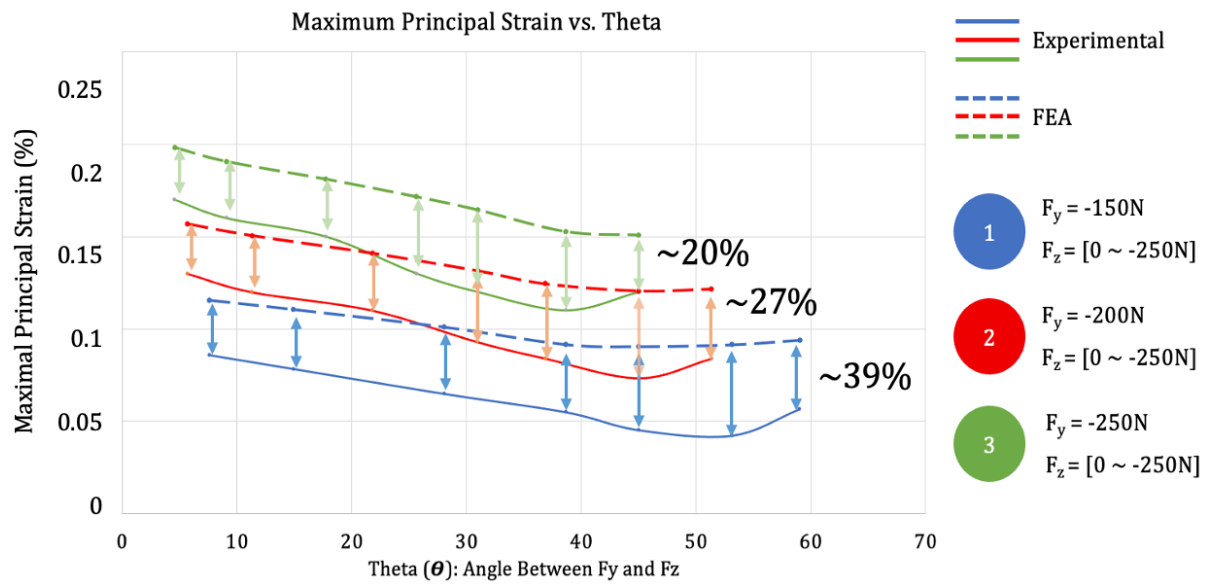


Figure 23. Average Percent Differences between FEA and Experimental Results: Solid line (Experimental), Dashed Line (FEA)

Chapter 6: Discussions

Both the FEA and the verification tests showed that there was a distinct and linear relationship between the maximum strain and angle between forces applied, as shown in Figure 22. When comparing the values of the strain found on the stump support, FEA showed generally higher strain values than those from the verification test.

Figure 23 shows a trend in which the percent differences between the FEA and experimental test decreased with increasing load applied to the stump support. This trend may also be related to how the athlete is using the stump support during cycling in relation to the pushing and pulling phase of the crank cycle. Further analyses are required to determine the reason for the observed trend. The trend did not impact the results but can be explored as a future study. Furthermore, the trend of these differences could not be verified as a limited number of masses were used. Further analyses with sufficient masses, such as the weight of the athlete, are required to investigate the significance of these differences and are required to verify the observed trend.

Furthermore, both the FEA and experimental results show that all the strain values for each component (ϵ_a , ϵ_b , ϵ_c) increased at a larger angle between forces, deviating from the general relationship of a linear decline. This increase in strain was observed when the magnitude of the force applied in the Z (transverse) direction was greater than that of the force applied in the Y (vertical) direction. Further increasing the magnitude of the forces in the Z direction up to 400N via FEA showed an increase in maximal principal strain, following the upward trend found at the end of the previous results. This characteristic strain response of the stump support indicated that the strain found on the stump support is direction-dependent, where the direction of the force applied to the stump support can be isolated to describe the method of force application by the para-cyclist.

Previous studies have noted that for able-bodied cyclists, the revolution of the crank during cycling is primarily directed by tangential force (F_T) that is applied perpendicular to the crank arm of a bicycle during the pushing phase of a crank cycle. Since the pedals are 180° out of phase with each other, this force contributes to

executing the rotation of the crank completely. However, for a single-legged para-cyclist with a stump support, the application of this tangential force (F_T) to crank the pedal is absent on the side of a residual stump. Based on the relationship between the direction of applied force and maximum strain, it can be theorised that a different type of force is applied onto the stump support to contribute to rotate the crank arm of the contralateral side of a bicycle. This different type of force may be related to the contribution of the force applied in Z (transverse) direction to rotate the crank rather than that of tangential force, predominantly.

6.1. Limitations

There were a significant number of limitations during this study, presented during both FEA and experimental testing, that may have affected the differences observed between the strain obtained from the FEA and experimental test results.

6.1.1. FEA Limitations

The assumption made regarding the material properties of the stump support model used in FEA may not accurately represent those of the actual stump support. Further studies are needed to investigate the material properties, such as elastic (Young's) modulus, and Poisson's Ratio, of the stump support and verify the FEA results.

6.1.2. Experimental Test Limitations

The method of applying the load onto the stump support was different to that of FEA. During the experimental test, forces were applied by adding different masses onto the basket that is held by a steel chain, wrapping around the front plate of the stump support. Having the chain wrapped around the front plate, the force was not applied at the vertex of the front plate, but rather distributed along the plate, and meeting at one concentrated point of a chain, resulting an applied force different than that of FEA. This method of force application is shown in Appendix E.

The effects of this loading method may have contributed to differences found between FEA and experimental test results as shown in Figure 23. However, it is estimated that such limitation would not impact the linear relationship between the maximum strain and the angle between bi-directional forces. This is because the force is translated to the

entire stump support, rather than one particular point as suggested in FEA. Thus, this relationship remains the same regardless of the location of the force applied. However, further studies, investigating the effect of changing the location of applied force, are required to verify the significance of this difference in the method of force application.

Also, it was only possible to apply a force up to 250N (25kg) due to the robustness of a steel chain with a basket, which is a third of the para-cyclist's body weight (75kg). There were no other viable methods of carrying the suggested weight during the experimental test. Applying additional loads to the stump support may strengthen the observed relationship between applied force and strain by providing a broader spectrum of a characteristic strain response.

Chapter 7: Future Work

Following on from this study, investigating the neuromuscular activation pattern of the healthy lower limb in relation to the crank cycle while analysing the strain determined on the stump support to synchronize these parameters with one another would be a valuable exercise. Synchronization of the neuromuscular pattern, and the strain found on the stump support in relation to the crank cycle can ultimately help describe the kinematics of single-legged para-cycling. Suggested experimental procedures of collecting neuromuscular and motion capture data are listed in Appendix G and H below. Also, the description of suggested experimental protocols for the participant is listed in Appendix I.

As previously mentioned, this study focused on developing a method that allowed for an analysis of the force applied to the stump support by the para-cyclist. This analysis can be achieved by investigating the strain found on the plate of a stump support rather than the actual prosthetic socket. The engineering file of the prosthetic socket component of the stump support allows for the strain across the surface of a prosthetic socket to be studied. This contributes to recognising the characteristic strain response of the stump support when a force is applied, further developing the understanding of the impact of the stump support in single-legged para-cycling.

Furthermore, the force applied by the contralateral leg on the pedal to rotate the crank can be investigated to describe the force application pattern during both the pushing and pulling phase in relation to the crank cycle. Additionally, the relationship between the pedal force and the force applied on the stump support should be investigated. As previously mentioned, current literature has noted the importance of applied force on the pedal and its relation to performance output. Exploring this relationship may contribute to understanding the effect of the stump support during cycling and the para-athlete's overall performance.

Chapter 8: Conclusion

This study aimed to develop a device that would allow for a rudimentary understanding of the kinematics of a single-legged para-cyclist using a stump support during cycling. Specifically, the derivation of force application done by the para-cyclist onto the stump support was inferred by measuring the strain found on the stump support. While current studies have noted the differences between the neuromuscular pattern of a single-legged para-cyclist and that of able-bodied cyclists, the same analysis has not been investigated for para-cyclists who use a stump support during cycling.

Both FEA and the experimental study showed that there is a linear relationship between the maximum strain and the angle between forces applied to the stump support. The establishment of this relationship further indicates that the force being applied to the stump support during cycling can be derived by analysing the strain on the stump support. This method will allow for identification of the direction that the force is applied onto the stump support. Furthermore, the comparison between the theoretical and experimental results showed that further analysis is required to investigate the significance of differences between the results.

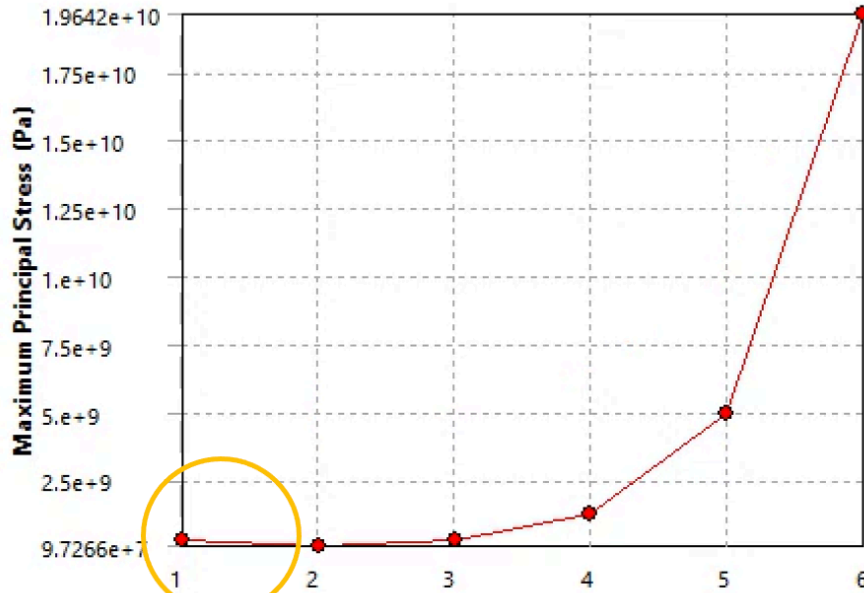
References

- [1] Hug, F, "Electromyographic analysis of pedalling: review," Journal of electromyography and kinesiology: official journal of the International Society of Electrophysiological Kinesiology, 2008, 19(2):182-98
- [2] Watanabe, K *et al.*, Neuromuscular activation pattern of lower extremity muscles during pedalling in cyclist with single amputation of leg and with two legs: a case study, BMC Research Notes, 2020, 13:299
- [3] Paralympics Australia, Classification Information Sheet, Union Cycliste Internationale (UCI), 2019
- [4] Lee, R, Simon, R., Relationship between starting and finishing position in World Cup BMX racing. International Journal of Performance Analysis in Sport. 2014, 14-23.
- [5] Jansen, and McPhee, J., "Predictive Dynamic Simulation of Seated Start-Up Cycling Using Olympic Cyclist and Bicycle Models," 2018, vol. 2, no. 6, p. 220.
- [6] South Australian Sports Institute (SASI), Training Protocol, Office for Recreation, Sports, and Racing (ORSR), 2021
- [7] Fonda, B., et al., Biomechanics of Cycling, Sport Science Review XIX, 2010, (1-2)
- [8] Raymond, C.H. Joseph, S, Ng, *, K.-F., Ng, G, "Muscle recruitment pattern in cycling: a review," Sports Science Department, Hong Kong Sports Institute, Physical Therapy in Sport 2005, 6: 89–96
- [9] Coyle, E.F et al., Physiological, and biomechanical factors associated with elite endurance cycling performance. Med Sci Sports Exercise. 1991 Jan;23(1):93-107.
- [10] Ericson et al., Power output and work in different muscle groups during ergometer cycling, *European Journal of Applied of Physiology and Occupational Physiology* 1987, 55, pg. 229–235
- [11] Holmes, D.P., Mechanics of Material: Strain, Boston University; Mechanics of Slender Structures, 2021.
- [12] Faria, E.W., et al., The Science of Cycling: Physiology and Training – Part1, Sports Medicine, 2005, 35(4):285-312
- [13] François et al., Force-velocity relationship in cycling revisited: benefit of two-dimensional pedal forces analysis, Medicine and Science in Sports and Exercise, American College of Sports Medicine (ACSM), 2010, 42 (6), pp.1174-1183.
- [14] Broker, et al., The biomechanics of cycling, Exercise and Sports Sciences Reviews, 1991, 19, 127-169

- [15] Hasson, CJ, et al., Changes in muscle and joint coordination in learning to direct forces. *Human Movement Science*, 2008, 27: 590-609
- [16] Ibrahim, et al. 2020, Effective thermal conductivity of 3D-printed continuous fiber polymer composites,
- [17] Kyowa Electronic Instruments Co. Ltd, Method of Obtaining Magnitude and Direction of Principal Stress (Rosette Analysis), 2021
- [18] Carinena, JF, et al., Superposition rules for higher-order systems and their applications, *Journal of Physics a Mathematical and Theoretical*, 45(18)

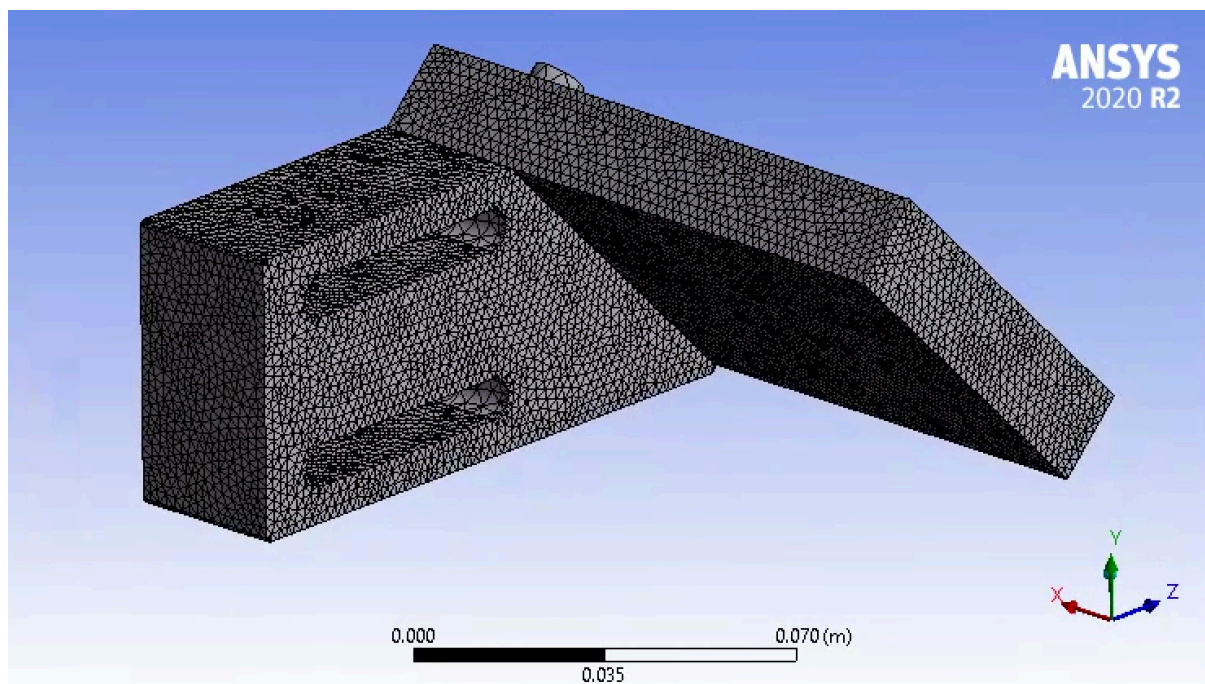
APPENDICES

Appendix A: Mesh Convergence Plot of the Stump Support Model



	Maximum Principal Stress (Pa)	Change (%)	Nodes	Elements
1	3.0253e+008		135790	77962
2	9.7266e+007	-102.68	209791	128583
3	3.4586e+008	112.2	422571	273743
4	1.3009e+009	115.99	777249	524821
5	4.9328e+009	116.52	1924154	1350491
6	1.9642e+010	119.71	3122119	2213575

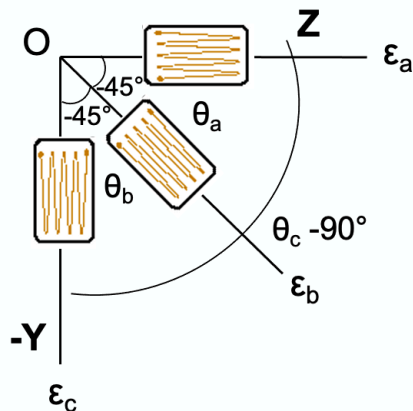
Appendix B: Mesh Analysis of the model with element size of 0.002m



Appendix C: Specification of the Kyowa Strain Rosette



Appendix D: Equations to Calculate: Maximum Principal Strain & Torsion of Individual Strain

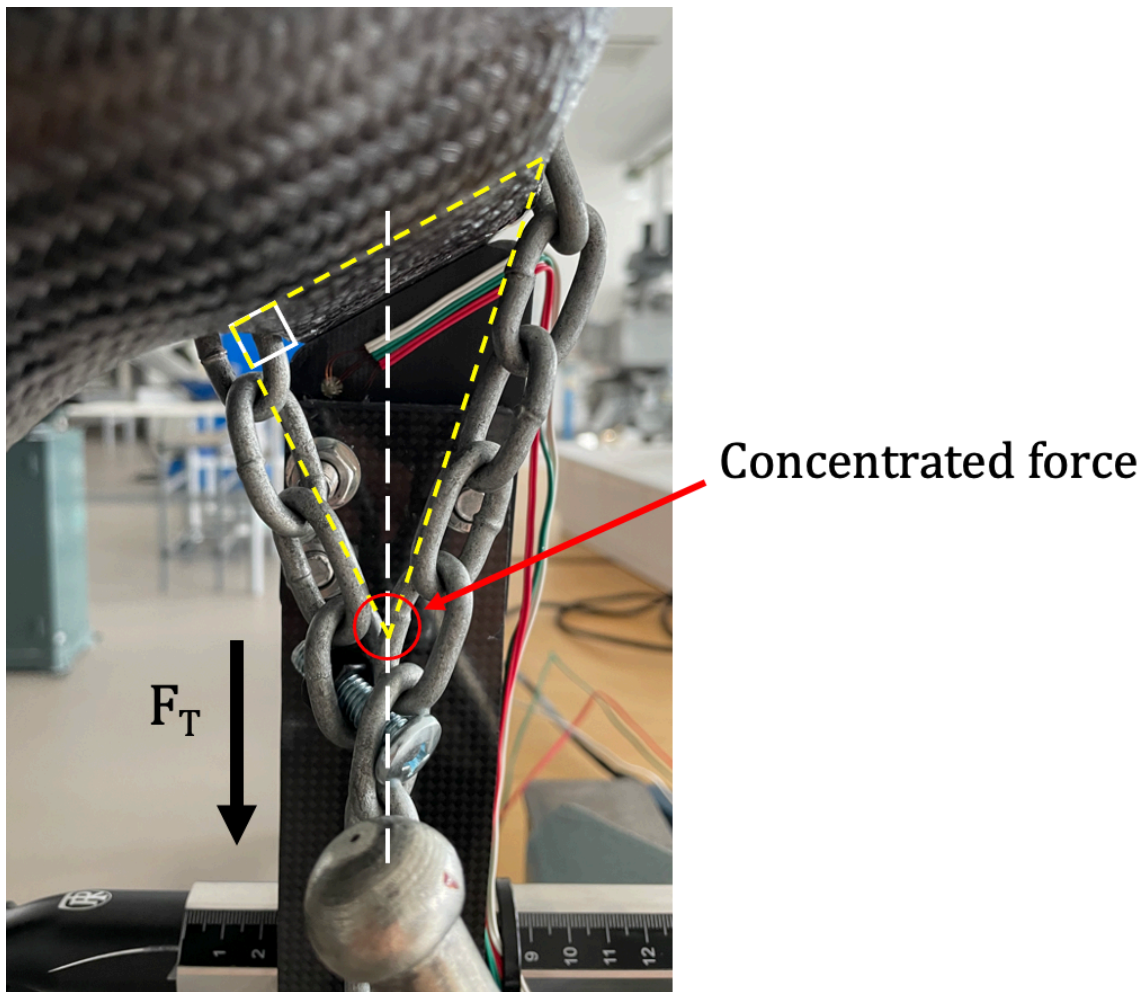


$$\epsilon_a = \epsilon_z \cos^2(\theta_a) + \epsilon_y \sin^2(\theta_a) + \gamma_{yz} \sin(\theta_a) \cos(\theta_a)$$

$$\epsilon_b = \epsilon_z \cos^2(\theta_b) + \epsilon_y \sin^2(\theta_b) + \gamma_{yz} \sin(\theta_b) \cos(\theta_b)$$

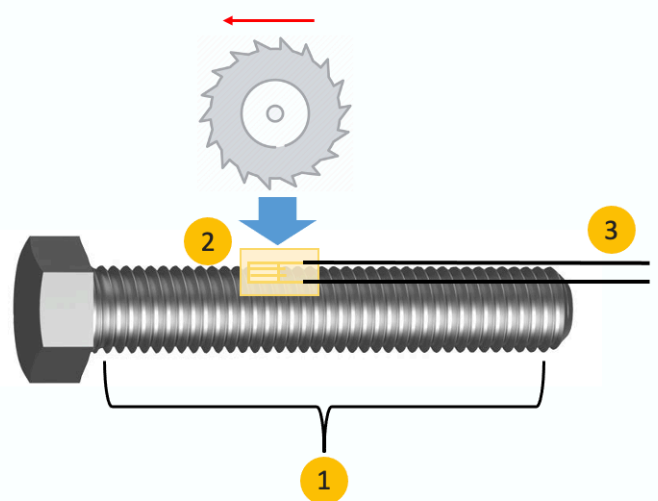
$$\epsilon_c = \epsilon_z \cos^2(\theta_c) + \epsilon_y \sin^2(\theta_c) + \gamma_{yz} \sin(\theta_c) \cos(\theta_c)$$

Appendix E: Method of Force Application in Experimental Testing



Appendix F: Physical Limitations of Sensor Placement on the Bolts

- 1 The bolt is fully threaded
- 2 Fully threaded shaft of the bolt affects sensor placement
- 3 Cable management requires physical alteration of the prosthetics



Appendix G: Lower Body Marker Placement

Table 1. Location and Description of Lower Body Marker Placement

MARKER	LOCATION	DESCRIPTION
LASI	Left ASIS	Left anterior superior iliac spine
RASI	Right ASIS	Right anterior superior iliac spine
LPSI	Left PSIS	Left posterior superior iliac spine (at the point where the spine joins the pelvis)
RPSI	Right PSIS	Right posterior superior iliac spine (at the point where the spine joins the pelvis)
LTHI	Left Thigh	Over the lower lateral 1/3 surface of the left thigh. On the line made by the left hip joint and knee marker.
LKNE	Left Knee	On the flexion-extension axis of the left knee
LTIB	Left Tibia	Over the lower 1/3 surface of the left shank. On the line made by the left knee and ankle marker.
LANK	Left Ankle	On the lateral malleolus along an imaginary line that passes through the transmalleolar axis
LHEE	Left Heel	On the calcaneus at the same height above the plantar surface of the foot as the toe marker
LTOE	Left Toe	Over the second metatarsal head, on the mid-foot side of the equinus break between fore-foot and mid-foot
RTHI	Right Thigh	Over the upper lateral 1/3 surface of the right thigh. On the line made by the right hip joint and knee marker.

Table 2: Method to Identify Muscle Belly of Lower Limb Muscles

Target Muscle	Location	Movement
Gluteus maximus	Gluteal region (superficial)	Extends the thigh
Biceps femoris	Hamstring (posterior)	Moves back of lower legs up and back toward the buttocks, as when kneeling; moves thigh down and back; twists the thigh (and lower leg) outward
Semimembranosus	Hamstring (posterior)	Moves back of lower legs up and back towards the buttocks as when kneeling

		moves thigh down and back; twists the thigh (and lower leg) inward
Semitendinosus	Hamstring (posterior)	Moves back of lower legs up towards buttocks as when kneeling moves thigh down and back; twists the thigh (and lower leg) inward
Rectus femoris	Quadriceps (anterior)	Moves lower leg out in front of body, as when kicking; assists in raising the knee
Vastus lateralis	Quadriceps (anterior)	Moves lower leg out in front of body, as when kicking
Vastus medialis	Quadriceps (anterior)	Moves lower leg out in front of body, as when kicking
Gastrocnemius	Calves (posterior)	Plantar flexes the foot; flexes knee when foot is dorsiflexed
Soleus	Calves (posterior)	Plantar flexes foot
Tibialis anterior	(anterior)	Dorsiflexes the foot; inverts foot; aids in support of medial longitudinal arch of foot

Appendix H: Experimental Setup

Participants

Competitive or elite level trans-femoral amputee cyclists, who use a stump support are subjected to be recruited in the study. Due to limited number such cyclists in the world, one elite level participant was recruited for the study.

Motion Capture System (VICON)

The experimental testing is completed at the Rehabilitation and Motion Analysis Laboratory at Flinders University in Tonsley. The laboratory is equipped with VICON motion capture system, Delsys wireless EMG system, and a cycling ergometer with a prosthetic socket attached, for participant/s to use.

Motion Capture system is driven by capturing the movement of motion capture markers, which are retroreflective material, placed on the participant's limbs. These

motion capture markers reflect the emitted infrared light from the cameras, which access the reflection and determine the position of the marker in 3D space.

Body Market Set

To determine the joint angles and relative position of the body in 3D space, the motion capture marker set is placed on the participant's limbs of interests. The limbs of interests are determined based on the objectives of this study, focusing on specific limbs that contribute to pedalling the bicycle crank. The placement of the market set (mirror image) is shown by blue and green dots in Figure 1 below:

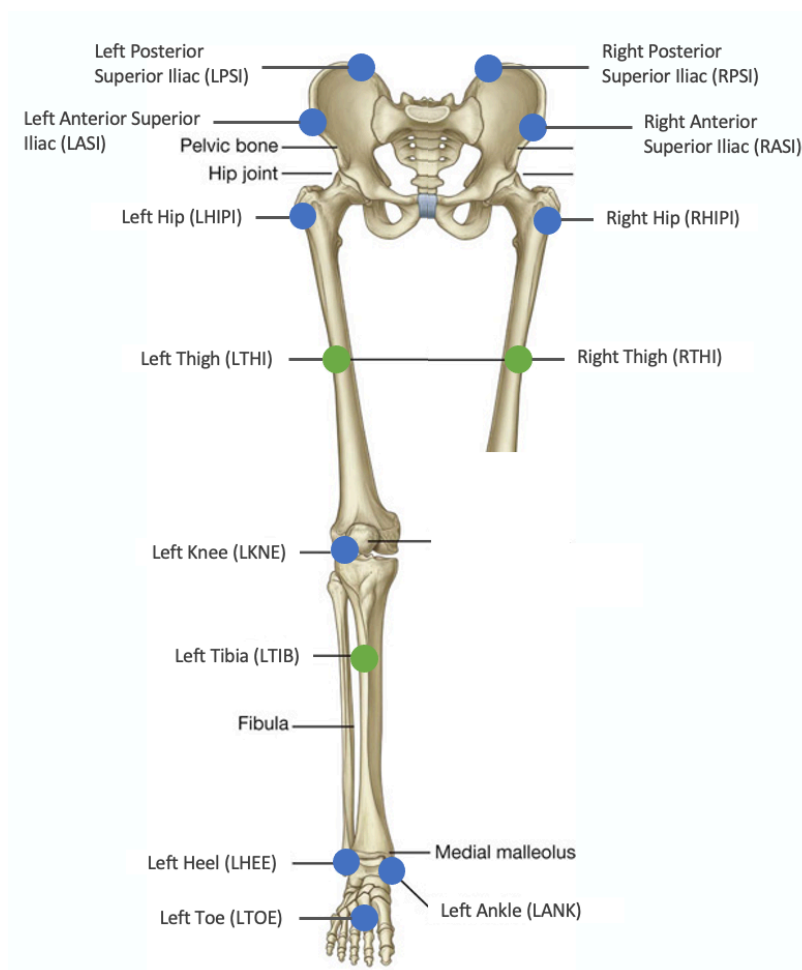


Figure 1. Motion Capture Body Market Set: Blue dots are placed on *bony landmarks* while green dots are placed on *soft tissue landmarks*.

Markers, indicated above, are placed both relative to the bony landmarks and soft tissue landmarks to ensure repeatability and accuracy of the measurement. The placement of these marker set, described on the VICON website, and the detailed description of each marker placement can be found in the Appendix G. Such placement of this marker set

provide angular data of hip, knee, and the ankle, as required for analysis of the crank cycle (ref).

Delsys Wireless EMG System

During this study, muscle activities were measured by Delsys Wireless EMG System. This EMG system consists of 16 wireless EMG electrodes with an example as shown in Figure 2 below. Each electrode was placed at the belly of the designated major muscles of lower limbs.

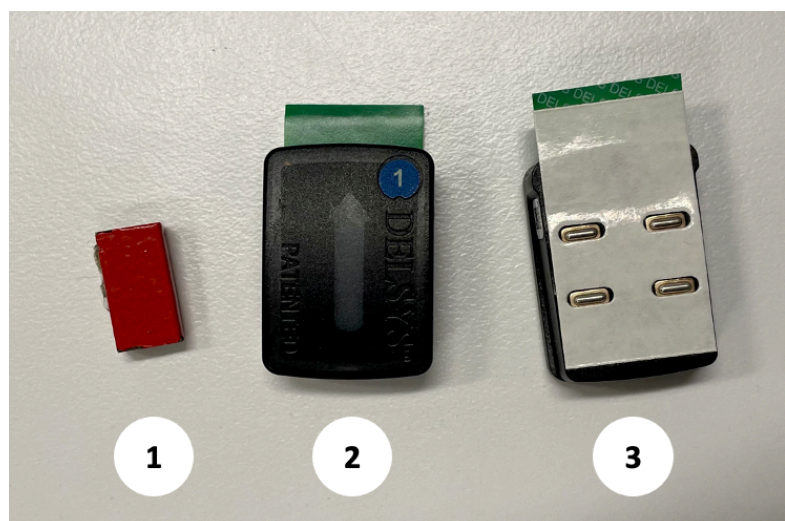


Figure 2. Delsys EMG electrode; an Arrow indicates suggested orientation of the electrode in relative to the direction of the muscle fibres. 1. a magnet to charge the electrode 2. front view of the Delsys EMG electrode 3. back view of the Delsys EMG electrode, showing sensor nodes

Pilot Study

A pilot study is conducted to determine optimal position of the ergometer relative to the camera setup. Also, this study is conducted to locate any possible data lost from the motion capture markers placed on the participant's limbs during data capturing. This is to ensure that data obtained during data capturing are reliable and repeatable.

Kinematic Setup

The VICON motion capture cameras are configured into the layout in the lab as shown in figure 3a, 3b below:



Figure 3a. VICON motion capture camera setup in real-time environment

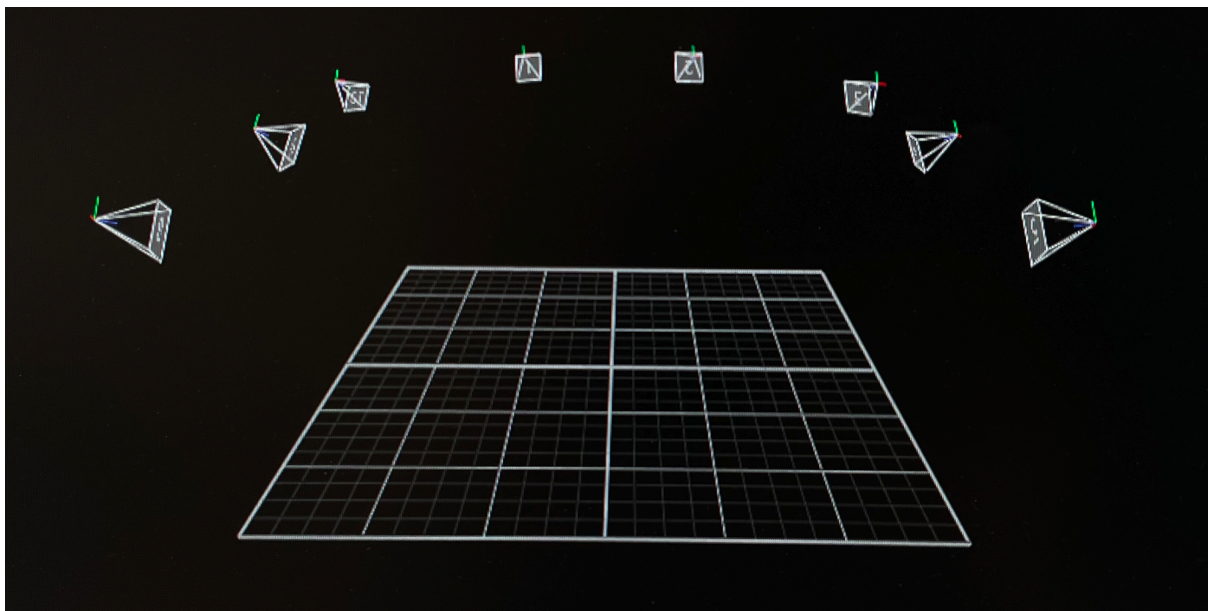


Figure 3b. VICON motion capture camera setup in virtual environment

Following the setup of the cameras, the motion capture marker set is placed on the lower limbs of the participant, and the X, Y and Z joint angles of the lower limbs were analyzed, using VICON Nexus software.

For the pilot study, the participant is, first, asked to start walking from the outside of the frame and onto the ergometer. This protocol is implemented to ensure that markers are populating correct joint formation. Loss of any data will obstruct the joint formation. Following this, the participant is asked to raise their hands above their head and bring them back down to mark the start time of the study. Upon completion of raising their hands, the participant was asked to ride the ergometer at a comfortable workload for 10

seconds. This is to monitor any possible marker loss at different position in the crank cycle, and the need for possible adjustments in camera position.

The pilot study populated the joint formation correctly, and no data was lost. *PlugInGait LowerBody Ai* data was used to build the joints of the lower limbs as shown in figure # below (Ref-Vicon Software).

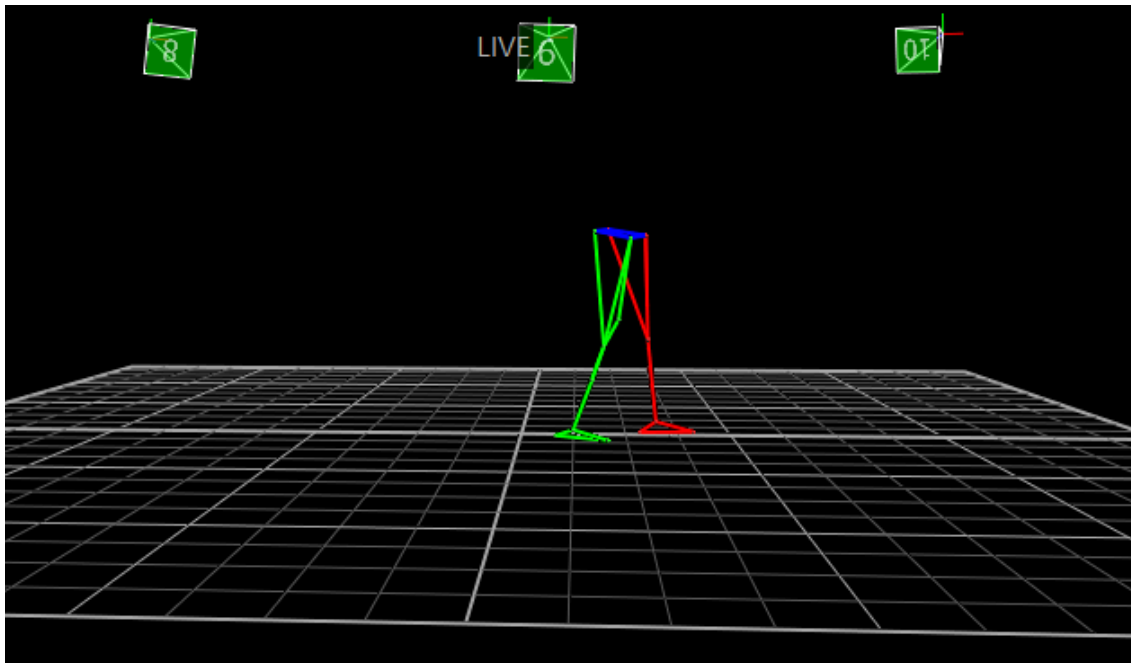


Figure 4. Motion capture marker setup for pilot study (lower limbs)

Experimental Setup

Following a standard procedure, the motion capture setup is calibrated using a standard technique. Following the calibration, the ergometer is set at the centre of the room as shown in figure # below:

The experimental procedure is verbally explained to the participant as well as the coach. A questionnaire sheet, aiming to qualitatively understand how the participant use the stump support, is provided to the participant prior to conducting the test for the participant to answer (Appendix #). Following this, a written consent form is provided for the participant to sign.

EMG Placement

A set of electrodes are placed on the belly, and in the direction of the following muscles as shown in figure #: gluteus maximus (G_{Max}), biceps femoris (BF-long head), semitendinosus (ST), vastus medialis (VM), vastus lateralis (VL), rectus femoris (RF), tibialis anterior (TA), medial gastrocnemius (MG), lateral gastrocnemius (LG), soleus (Sol). For RF muscle, proximal (RF_p) and distal (RF_d) regions of the muscle were recorded.

Motion Capture marker Placement

The motion capture markers are placed on the participant's lower limbs. One marker is placed at the tip of the participant's footwear to obtain positional data of the pedal relative to the crank cycle.

Appendix I: Experimental Protocol

The prosthetic socket is mounted on the bike seat with participant's usual setup as shown in figure 5. The participant performed his/her usual training warm-ups on an ergometer provided. These warm-ups are not specified nor deviate from his/her regular training routines to avoid any confounding factors. Following the warm-ups, the participant was asked to take a 2-minute rest, which mimicked the athlete's standard recovery period. The participant performed one of his/her regular training routines: three sets of Six-second Burst.

3 Sets of 6-Second Burst

This testing protocol is one of the participant's standard trainings, which entailed the participant cycling on a SRM unit at specific cadence. The start of the trial was indicated by the participant, raising both of his hands above his head, and bringing back down. This ensured that the VICON and EMG data could later be synchronized during data analysis. The cadence level was set at 150 rpm, ensuring that each trial contained at least six crank revolutions with a total of 15 revolutions based on the observation of the healthy limb. Following the end of each trial, the participant was asked to rest for five minutes with a choice of comfortable setting.